Journal of Applied Fluid Mechanics, Vol. 17, No. 1, pp. 176-191, 2024.
Available online at www.jafmonline.net, ISSN 1735-3572, EISSN 1735-3645.
https://doi.org/10.47176/jafm.17.1.1978

Numerical Investigation of Lucid Spherical Cross-Axis Flow Turbine with Asymmetric Airfoil Sections and the Effect of Different Parameters of Blades on Its Performance

H. Zarei and M. Passandideh Fard†

Ferdowsi University of Mashhad, Department of Mechanical Engineering, Mashhad, Iran

Corresponding Author Email: fard_m@um.ac.ir

ABSTRACT

The numerical investigation has been performed on the cross-axis-flow lucid spherical turbine. This type of cross-axis flow turbine generates moments through the forces acting on its blade cross-sections. To evaluate its power and performance, a three-dimensional simulation procedure was performed. The experimental results of Bachant and Wosnik have been used to verify the numerical predictions. The spherical lucid model turbine which they examined had 4 blades with NACA 0020 section and 16cm chord length. Drag and power coefficients were used to compare the data for the water inlet velocity 1m/s and different non-dimensional tip-speed-ratio (inlet velocity / linear rotating velocity of the blade). This paper has selected two airfoil sections, NACA 2412 and NACA 64(3)418, to design the turbine blades. The influence of four effective blade parameters, inclusive of profile section type, chord length, number of blades, and blade twist angles, on turbine performance over a wide range of tip speed ratios, is investigated. It can deduce that the power coefficient has increased up to 22% for NACA 2412 compared to the experimental test. Also, the three-bladed turbine possesses the best results among all models. For this model, the power coefficient increased by 12% and 71% for NACA 2412 and NACA 64(3)418 sections, respectively. The twist of the blades increases the power coefficient by 19% and 31% for NACA 2412 and NACA 64(3)418 sections inside the channel respectively. Increasing the blade chord length causes to increase in power coefficient of up to 12% for NACA 2412 section compared to the experimental test.

Article History

Received May 17, 2023
Revised August 6, 2023
Accepted September 12, 2023
Available online November 1, 2023

Keywords:

Lucid spherical turbine
Drag coefficient
Power coefficient
Helical turbine
Asymmetric airfoils

1. INTRODUCTION

Renewable energy technologies play an important role in helping to achieve sustainable energy. These technologies will eliminate our dependence on fossil fuels and pave the way for sustainable and pollution-free energy security. Interest in using marine currents as a sustainable energy source has been growing over the past year. For extra-low head hydropower utilization, the Darrieus-type hydro turbine system has been suggested (Furukawa et al., 1992). The Darrieus vertical axis slide with two-dimensional blades is so simple that it has the cost benefit. Moreover, if the head is low, only the radius R of the rotating pitch circle or the duct height B can be modified in proportion to the available flow rate, which is another advantage of Darrieus Runner (Shimokawa et al., 2012).

A lift-type hydro turbine developed by Lucid Energy Inc. having a diameter of over 600 mm and a flow velocity of more than 3 m/s. The goal of this design is to maximize the water energy extraction from the rotor (Yang et al., 2019). The Darrieus type's low start-up torque can be a disadvantage. To address this issue, researchers have developed a variety of dimensionless rotor parameters that can be used to improve their performance.

In current years, numerous studies have shown that a high solidity ratio can improve the start-up torque and the self-starting capabilities of a Darrieus vertical-axis wind turbine. However, the diverse effect of high solidity

NOMENCLATURE

A	cross-sectional area of the stream tube	C_d	drag coefficient
A_2	turbine frontal area	C_P	power coefficient
U_1	inlet velocity	***Greek symbols***	
U_2	velocity before the disk	ρ	fluid density
U_3	velocity after the disk		

on the coefficient of performance has been reported. To improve the efficiency of this type of turbine, a team of computational fluid dynamics experts conducted a first-of-its-kind simulation of the dynamic motion of a blade. By simulated the dynamic motion of a turbine blade spinning about a vertical axis and subjected to a far-field uniform free-stream velocity flow field (Balduzzi et al., 2020). (El Chazly, 1993) performed static and dynamic FEM analysis of horizontal-axis wind turbine blades made of NACA 0015 symmetrical airfoils (Castelli et al., 2013).

Tunio et al. (2020), recently studied the impact of pitch angle and blade profile on the hydro-kinetic performance of the Darrieus turbine. The discovery was made that the blade with NACA0020 air-foil at A 4-degree pitch angle model is more efficient than a NACA 0015 with a blade profile that is higher. They also noted that a zero-degree pitch angle turbine is more superior to a turbine with a higher pitch angle in terms of performance. (Alaimo et al., 2015), evaluated the aerodynamic performance of helical and straight-bladed vertical axis wind turbines. They discovered that despite the fact that electricity generation by way of a helical rotor was decrease, its overall performance was more stable as compared to a straight-bladed one, to predict the output energy of a helical wind turbine in numerous tip speed ratios (Moghimi & Motawej, 2020).

Li et al. (2021), the focus was on the power output of vertical axis wind turbines with different blade numbers in a large wind tunnel that have a six-component balance. It is evident that the power coefficient's maximum value increased as the number of blades decreased, while the tip speed ratio decreased. However, most of the above studies were limited to the power and torque coefficients (Li et al., 2021). The increase in angle of attack causes dynamic stall to occur more frequently at lower blade tip speeds. Tirandaz and Rezaeiha aimed to study the effect of airfoil shape on a dynamic stall, as there are hardly any research reports demonstrating the phenomenon. Their study of 126 airfoils with different shapes revealed that increasing the leading-edge radius results in a decrease in power coefficient in all cases, the turbine performance can be improved by increasing the blade thickness at low blade speeds, but it was not observed at high blade speeds. (Ghiasi et al., 2022).

The influence of turbulence in the wake was studied by, Peng, H. for a five-bladed vertical axis wind turbine, recording better self-starting capabilities and a lower speed deficit in the far wake; also recorded faster wake recovery for a three-bladed turbine (Hohman et al., 2018). Results of (Hwang et al., 2009) and (Paillard et al., 2013) with pitching blades and (Antheaume et al., 2008). The forces exerted by the fixed blades on the turbines' rotor blades can negatively affect their performance. In addition, the dynamic stall and blade wake can also cause cyclic disturbances in the rotation of the turbines. Vortex triggering isn't taken into account when it comes to these types of turbines' wake interactions. (Gorle et al., 2015). (Dashti Mahmoud-abadi et al., 2022) performed a three-dimensional steady numerical simulation to determine a lucid spherical turbine with a symmetric NACA 0020 blade for low velocities in a channel.

Lucid turbines are a kind of cross-axis flow that generate moments via lift forces imposing on blade cross-sections. Spherical Lucid turbines consist of several circular blades with symmetrical or asymmetrical profile sections that rotate around the center line perpendicular to the free incoming water flow. Thus the angle of attack for all blades varies in time even for steady flows. Steady three-dimensional simulations have been employed to evaluate the performance and power of this kind of turbine in a channel with low velocity. The present research aims to know the proper parameters range influencing the turbine design, such as the number of blades, chord length, and airfoil type, to increase turbine performance at low speeds.

The innovations of this research include the change in the number of turbine blades, which led to better performance in the turbine with the number of three blades. Also, the twisting of the turbine blades is another novelty of this research, and it was found that the turbine performs better in negative twisting angles. To identify the twisting angles of the blades used in the research, several numerical experiments have been done. Finally, the effect of increasing chord length on turbine performance was investigated.

2. AERODYNAMIC PERFORMANCE

The propeller was designed by Rankine based on the movement of water through the propeller disc. However, since his theory did not directly connect the geometry of the propeller to the thrust production, it was not used for the design of the actual propeller. Although it provides a general explanation of the efficiency of the propeller, it does not directly address the issue of power coefficient. Rankine's original theory was based on the following assumptions:

1. The propeller's operation in an ideal fluid prevents it from experiencing energy losses from frictional drag.

2. An actuator disc can replace the propeller, which is equivalent to stating that the propeller has an infinite number of blades.

3. Without causing rotation in the slipstream, the propeller can produce thrust (Carlton, 2018).

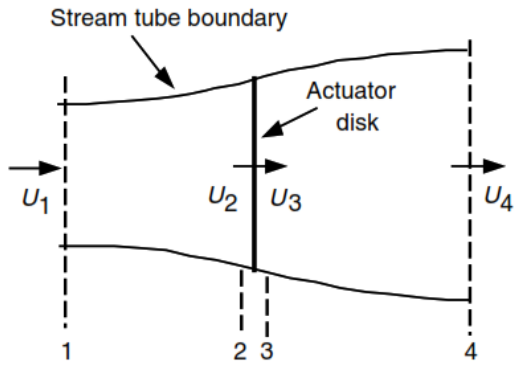

Fig. 1 Actuator disc model of a wind turbine; U, is mean air velocity; for different locations (Manwell et al., 2010)

The optimal shape for wind turbine blades is calculated using the concept of momentum and blade element theory. The results show that the general blade shape is derived from this approach. The two theories are then combined to create the blade element momentum or strip theory, which provides a procedure for analyzing the aerodynamic performance of a wind turbine (Manwell et al., 2010). A simple model, commonly credited to Betz (1926), the power output from an ideal turbine rotor can be assessed by using this method. The influence of rotor performance on the local wind field and the wind thrust on the ideal rotor. The thrust can be expressed as the net sum of the forces on each side of the actuator disc (Manwell et al., 2010):

$$T = A_2(P_2 - P_3)$$

If one solves for $(P_2 - P_3)$, obtains:

$$T = \frac{1}{2}\rho A_2(U_1^2 - U_4^2)$$

U_1, is the free flow velocity, A is the surface area of the tube, and A_2 is the turbine's anterior surface. The velocities just ahead and back of the propeller, U_2 and U_3 are the same to comply with continuity because the propeller is considered to be extremely slim. To reduce the solution, the conception of a flow stream induction factor is presented (Bachant & Wosnik, 2015):

$$a = \frac{U_1 - U_2}{U_1}$$

Hence flow velocity near the propeller is:

$$U_2 = (1 - a)U_1$$

To find the solution to wake recovery:

$$U_4 = (1 - 2a)U_1$$

The drag coefficient is to be represented in terms of the stream flow induction factor (Bachant & Wosnik, 2015):

$$C_d = \frac{F_d}{\frac{1}{2}\rho A_2 U_1^2} = 4a(1 - a)$$

Wind turbine rotor performance is usually characterized by its power coefficient, CP (Li et al., 2021):

$$C_P = \frac{U_2(U_1^2 - U_4^2)}{U_1^3} = 4a(1 - a)^2$$

3. TURBINE SPECIFICATION

The turbine that was tested was made by Lucid Energy Technologies. Details about its construction and sketches can be found in Table 1 and Fig. 2. (Bachant & Wosnik, 2015).

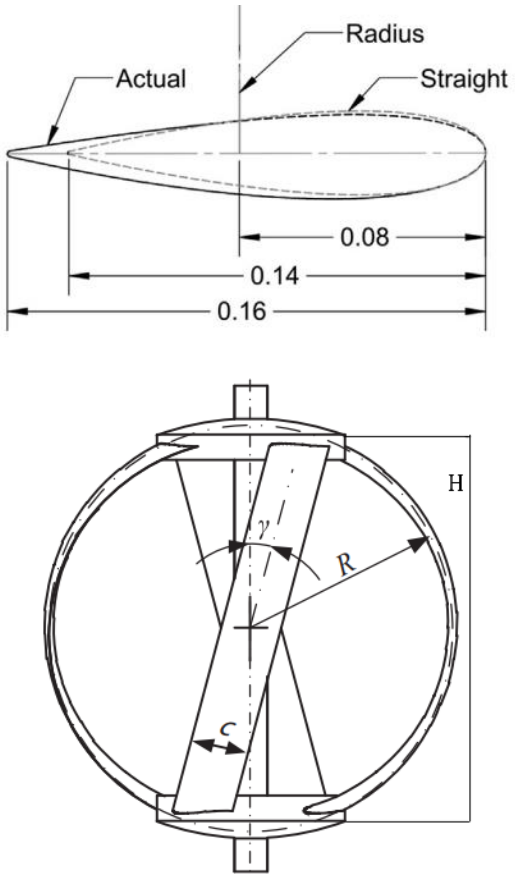

Fig. 2 Lucid spherical turbine with NACA 0020 foil section with 16 cm chord length manufactured by Lucid Energy Technologies (Bachant & Wosnik, 2015)

Table 1 Turbine Parameters (Bachant & Wosnik, 2015)

	LST
Diameter (m)	1.14
Height (m)	0.97
Frontal area (m2)	0.96
Blockage ratio	0.11
Number of blades	4
Equatorial solidity	0.18
Average solidity	0.22
Blade profile	NACA 0020
Blade overlap	2.0

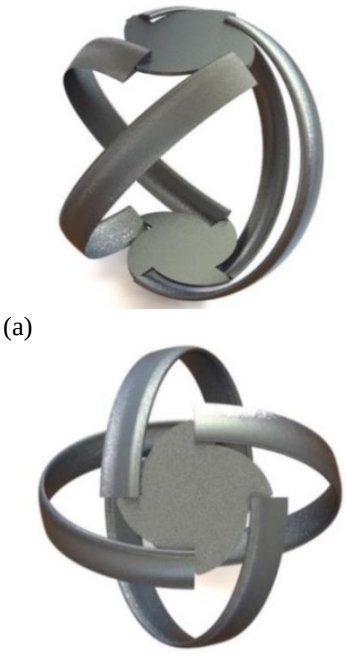

(a)

(b)

Fig. 3 Main design of the lucid spherical turbine by Solid-works software (a) Isometric plane and (b) Top plane

Figure 3 shows the lucid spherical turbine designed by Solidworks software. To design the turbine model Solid-works software was used. First, we produced the profile section, afterward using the Sweep technique the semi-circular blades were formed. Further, for the Hub section, the Extrude technique was applied, and then the blade and Hub parts were recalled and then assembled.

4. SIMULATION TESTBED DESIGN

Figure 4 presents the three-dimensional test bed of a lucid spherical turbine applied for CFD simulation. The CFD simulation geometrical model was developed for the turbine with 36.6 m long, 3.66 m wide, and 2.44 m deep. The lucid turbine was mounted approximately in the center of the model cross-section.

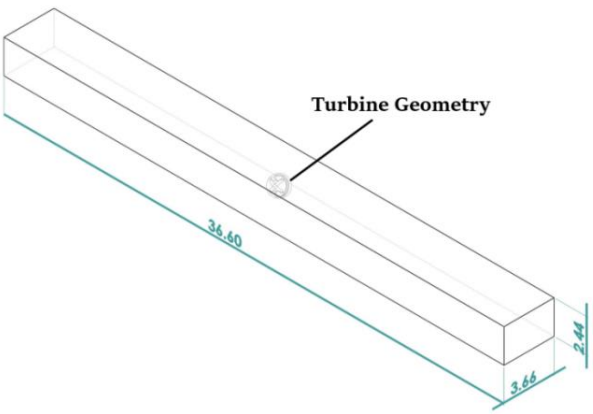

Fig. 4 Three-dimensional of a lucid spherical turbine Geometrical model for CFD simulation

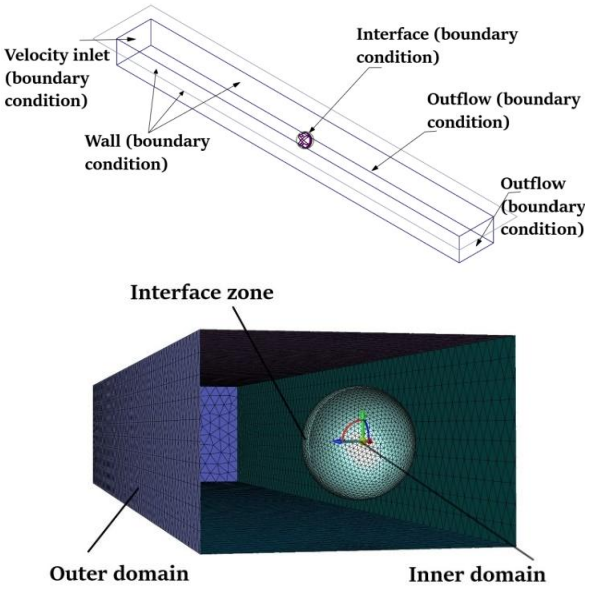

Fig. 5 CFD simulation Boundary conditions

5. SIMULATION METHOD AND BOUNDARY CONDITIONS

According to Bachant and Wosnik's experimental research, a numerical solution test bed is made. They tested a turbine in a channel with a low inlet velocity there was a wall around the channel, free atmospheric conditions prevailed above the channel, and the flow was directed out of the channel through an outlet.

To simulate the flow two-zone domains are assumed, the inner includes the turbine, and the outer domain includes the channel wall and inlet and outlet boundaries. For the inlet boundary a uniform velocity profile and for the outlet the outflow condition has been imposed, while for the left and right sides and down of the channel the wall condition, and for the upper boundary the outflow condition has been used.

Using the boundary condition of the outflow reduces the required time and memory. Although this condition is not completely accurate, considering the flow geometry and the distance considered for the upper boundary, it is close to reality. For this reason, the obtained results are acceptable compared to the experimental values. It is worth mentioning that for the use of this boundary condition if a higher height is considered for the channel, the results are slightly improved, due to the three-dimensionality of the field, it is not economical in terms of the time required to solve it.

To simulate the fluid flow the ANSYS-FLUENT software 2021 has been used. The Rotating-Frame method has been employed to rotate the rotor around the axis. In this method, the governing equations are solved in a reference coordinate that rotates with the rotor. The outer boundaries and also the rotor is fixed, but the axis-coordinates rotate in the opposite direction of the rotor. Figure 5 presents the CFD simulation boundary conditions. To perform the simulation, the

second-order spatial discretization and the first-order SIMPLEC temporal discretization algorithm are used. For convergence of the solution, momentum, drag, and turbine power coefficients are evaluated.

6. TURBULENCE MODEL

Recent studies on the design of turbines have shown that the SST K - ω turbulence model can be used to simulate vortical and fully turbulent flows. It has also been observed that the model performs well in the separation of flow and adverse pressure gradients. The SST model is based on combining two different turbulence models: the k–ω model in the inner parts of the boundary layer, and the k–ε model in the free stream. In 1993, Menter published a new k - ω -SST (shear stress transport) model which has remarkable advantages when compared with Wilcox's model or the k – ε model. In Menter's model, the k – ω equations are solved only inside the boundary layers, and the standard k – ε model is utilized elsewhere because the k – ε model is known to be insensitive to free-stream turbulence. He transformed the standard k - ε model into the k - ω form and developed a blending function F1 that equals one in the inner region and goes to zero near the edge of the boundary layer (Hellsten et al., 1997). The resulting new equations for k and ω are as follows:

$$\frac{\partial}{\partial t}(\rho k) + \frac{\partial}{\partial x_j}(\rho k u_j) = P - \beta^* \rho k \omega + \frac{\partial}{\partial x_j}\left(u + \sigma_\omega \mu T \frac{\partial k}{\partial x_j}\right)$$

$$\frac{\partial}{\partial t}(\rho\omega) + \frac{\partial}{\partial x_j}(\rho\omega u_j) = \frac{\gamma\rho}{\mu T} P - \beta\rho\omega^2 + \frac{\partial}{\partial x_j}\left(\mu + \sigma_\omega \mu T \frac{\partial \omega}{\partial x_j}\right) + 2\rho(1-F1)\frac{\sigma_{\omega 2}}{\omega}\frac{\partial k}{\partial x_j}\frac{\partial \omega}{\partial x_j}$$

Where ω is specific dissipation of turbulence kinetic energy, ρ is density, σ_ω represent turbulence-model constants, β, β^*, γ turbulence-model constants, μT is turbulent viscosity and F1 is auxiliary functions in turbulence model (Hellsten et al., 1997).

7. MESHING

Meshing and using a high-quality grid in numerical simulation is extremely important. A low-quality mesh can cause divergence and even reduce the correctness of the answers obtained from the simulation. Therefore, creating a high-quality mesh, generally for complex geometries, is one of the simulation topics in computational fluid dynamics. In the numerical simulation, the orientation of elements is sometimes fundamental in general, when the direction of the elements and the flow align, it causes to increase in the solution accuracy. Of course, it cannot predict the flow direction due to the existence of eddies or rotating flows. Fluent Meshing software was exerted, for the grid of the turbine geometric model in this research. A non-structured grid adapted for the outer and inner domains of the simulation, (Figs 6 and 7). An issue with non-structured mesh is the transition zone (the region between

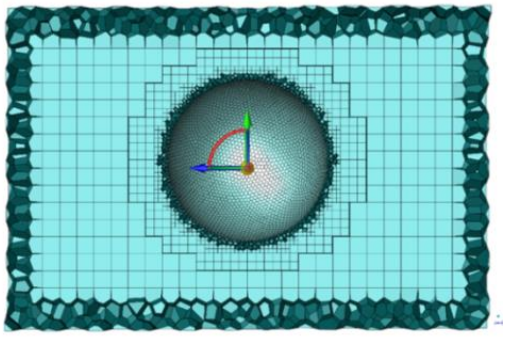

Fig. 6 Structured\non-structured grid adapted for outer domain and interface boundary condition

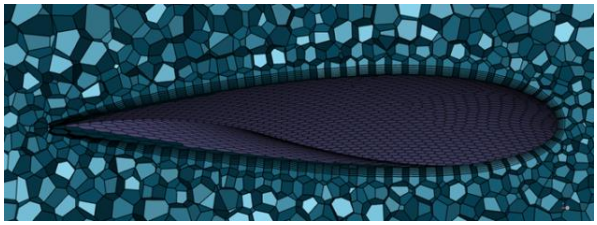

Fig. 7 Non-structured and boundary layer grid generated for the inner domain and near the turbine wall

boundary layer cells and volume cells). The Fluent meshing software uses hexagonal meshing to solve this problem. Using this technique, the number of elements reduce. The quality of the mesh is higher than in other meshing methods (Fig.7).

Structured mesh generally provides higher convergence for simulation due to better orientation in the computational area. When the geometry of the model is complex, it is no longer practicable to use structured meshing and is required to use unstructured meshing. Orthogonality is the angle ratio between two elements. Skewness is a measure that the closer to 1, the meshing is of lower quality, and the closer the orthogonality value is to 1, it means that the meshing has an extra good quality. In a meshing, we can consider both criteria. The quality and specifications of the mesh created on the 3D model of the turbines are presented in Table 2.

Five grids including 500 and 750 thousand, 1, 1.5, and 2 million cells are generated and the drag coefficient of the turbine is checked (Table 3). It was found that the grid with 1.5 million cells is satisfactory.

The fundamental meshing parameters that affect the numerical investigation are the number of boundary layer cells, the non-structured mesh growth rate, and the height of the first cell of the boundary layer. The mesh analysis has been done operating the k-ω SST turbulence model. Figure 9 shows that the y+~1 wall is satisfied for the test case.

Table 2 Quality of the cells

Number of cells	1,500,000
Orthogonal quality	0.95
Average skewness	0.37

Table 3 Drag and power coefficient for five values of mesh growth rate

Number of cells	Cd	Cp
500000	0.74893	0.1345
750000	0.77465	0.14657
1000000	0.8031	0.15748
15000000	0.82862	0.16428
20000000	0.83057	0.16683

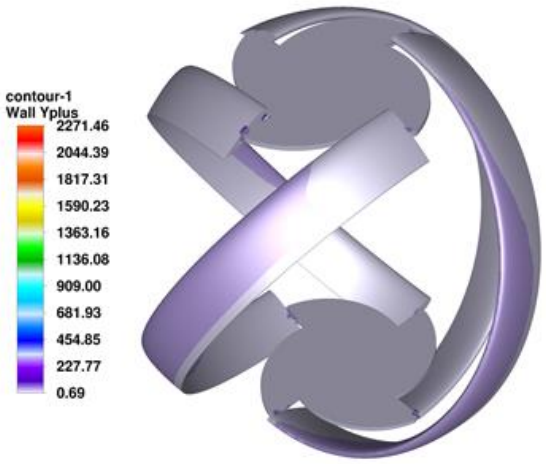

Fig. 9 Contour of Mesh study using the k-ω SST turbulence model

8. VALIDATION OF THE NUMERICAL SOLUTION WITH THE EXPERIMENTAL DATA

The experimental results of Bachant and Wosnik have been used to verify the numerical predictions. The spherical lucid model turbine that they examined had four blades with NACA 0020 section and 16cm chord length. Drag and power coefficients have been used to compare with the data for the water inlet velocity 1m/s and different non-dimensional tip-speed-ratio (inlet velocity / linear rotating velocity of a blade). The results in Fig.10 and Fig.11 show that the maximum deviation from the experiments for the drag coefficient is about 8%, while the power coefficient is 7%.

9. BLOCKAGE CORRECTION

Power coefficients, drag coefficients, and tip speed ratios were corrected for blockage using the method outlined in Appendix A of Bahaj et al. This method uses an actuator disk approach, taking into account the blockage ratio and drag coefficient to solve for an equivalent free flow velocity U_f, λ, C_P, and C_d are corrected as (Bachant & Wosnik, 2015):

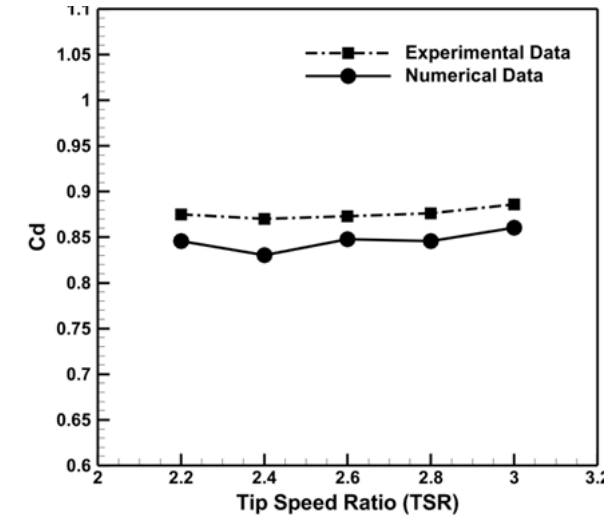

(a)

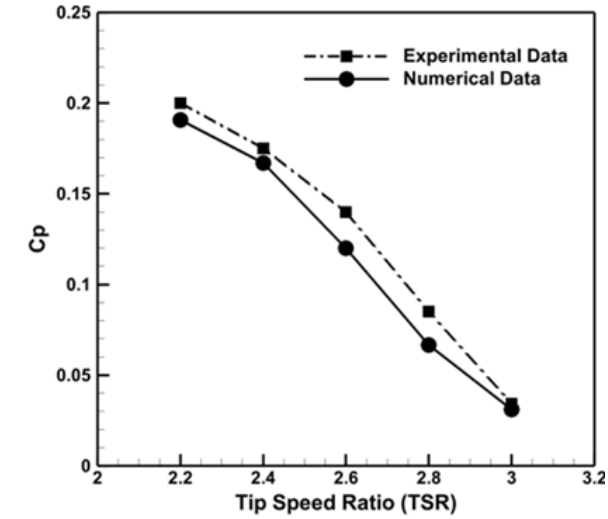

(b)

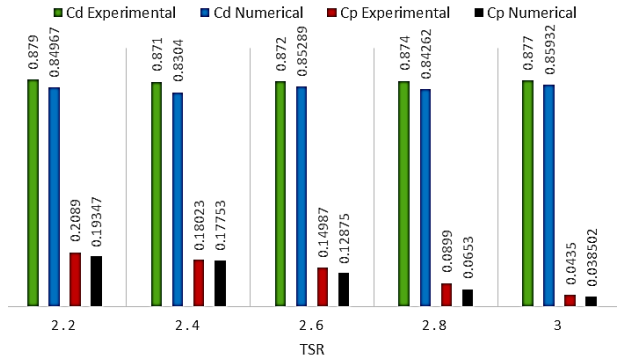

(C)

Fig. 10 Comparison of a) drag and b) power coefficient and c) error bar of numerical data and experimental research

$$\lambda_{Corrected} = \left(\frac{U_1}{U_f}\right)\lambda_{blocked}$$

$$C_{d\ Corrected} = \left(\frac{U_1}{U_f}\right)^2 C_{d\ blocked}$$

$$C_{p\ Corrected} = \left(\frac{U_1}{U_f}\right)^3 C_{p\ blocked}$$

Blockage-corrected drag and power coefficients are represented in Fig. 11. The plots show that the maximum deviation from the experiments for the drag coefficient is about 7%, while the power coefficient is 6% respectively.

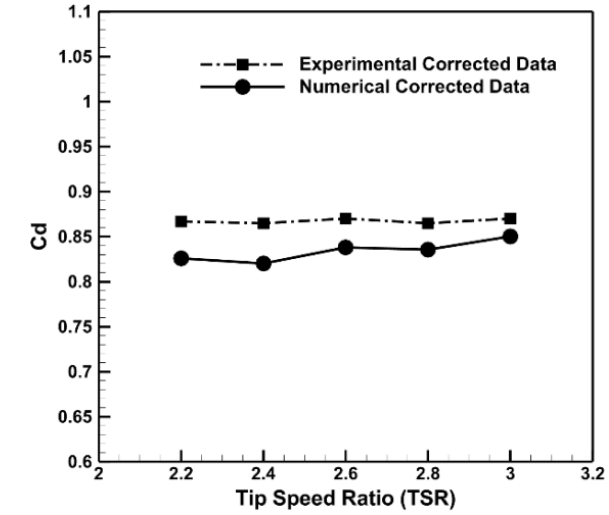

(a)

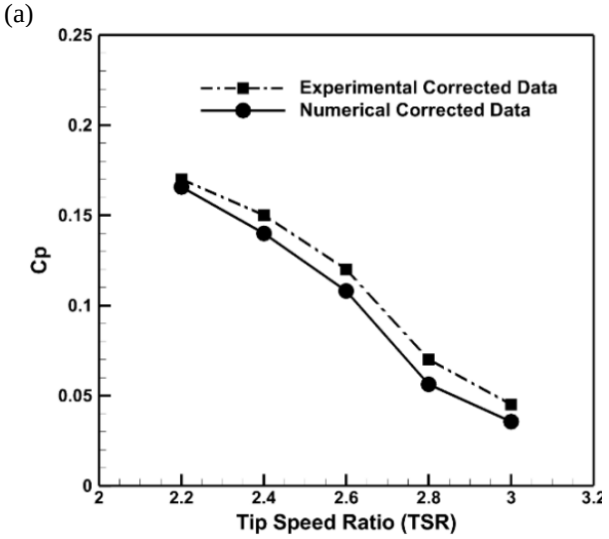

(b)

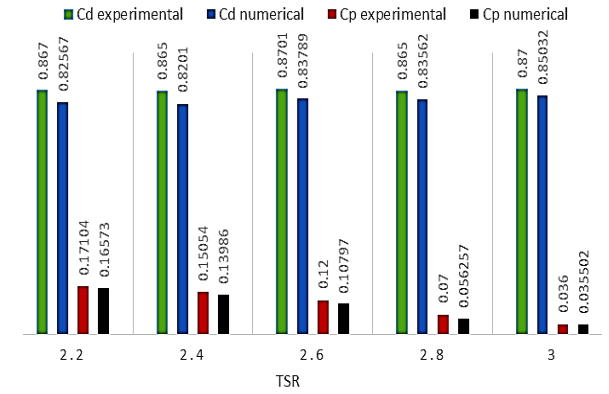

(C)

Fig. 11 Comparison of a) drag, b) power coefficient and c) error bar of experimental corrected data and numerical corrected data

10. RESULTS

10.1 Performance Analysis of Lucid Spherical Turbine with Asymmetric Airfoils

In this investigation, two airfoils, NACA 2412 and NACA 64(3)418, are selected to design the turbine blades. As can be seen in Fig.12, using NACA 2412 and NACA 64(3)418, sections show that the drag coefficient in all speed tip ratios is higher than the original turbine and has an increasing trend with increasing λ. For NACA 2412 and NACA 64(3)418, the maximum deviation from the original turbine drag coefficient is about 48% and 43%, respectively. Increasing the drag coefficient, which is opposed to driving the turbine onward, has decreased the turbine power coefficient. For NACA 2412, the maximum deviation from the original turbine power coefficient is about 15%. However, for NACA 64(3)418, it was found, that an increase in speed tip ratios causes to increase in the power coefficient of up to 17% compared to the original version.

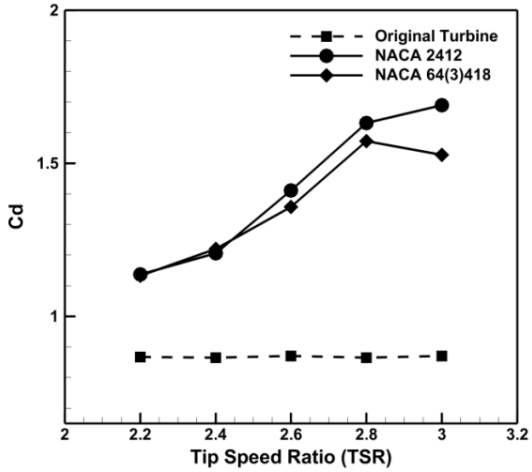

(a)

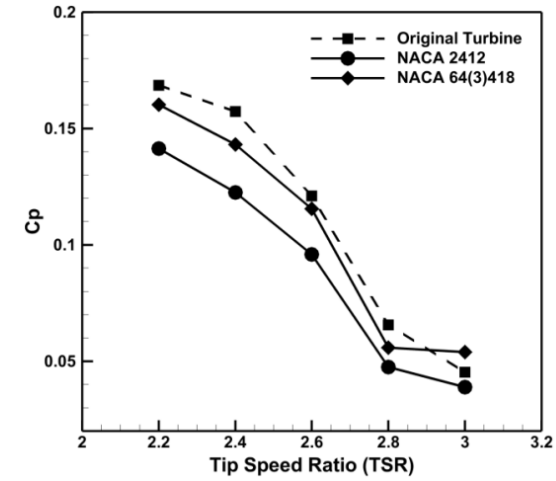

(b)

Fig. 12 (a) Drag and (b) power coefficient at different tip speed ratios for Lucid turbine designed by NACA2412 and NACA 64(3)418 airfoils compared with the original turbine

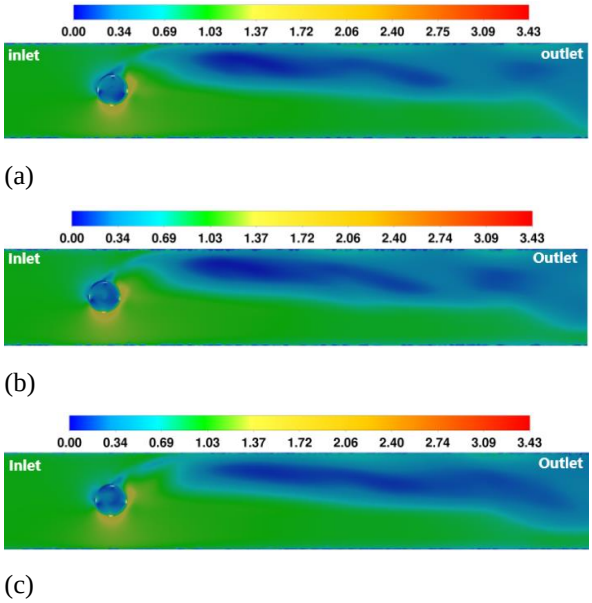

Fig. 13 Contours of streamwise velocity distribution in a horizontal plane at λ=2.2, (a) NACA 0020 (b) NACA 2412, and (c) NACA 64(3)418

Figure 13 illustrates the contours of the velocity in the streamwise direction in the horizontal planes, in various tip speed ratios, and the flow field. The turbine is mounted in a velocity domain with an angle of 90° to its rotation axis, the blade undergoes a force parallel to the turbine's rotation, which produces torque, and the turbine shifts forward. The sequential shift in the angle of attack causes to circulate the flow, which continually changes over the blades, forming a vortex. Two pairs of stall vortices formed. One of them is initiated on the leading edge, and the second vortex establishes on the trailing edge and spins in the contrary direction. Simultaneously, they create vortices rotating in opposite directions, which move downstream of the turbine. These vortices form a wave that disorganizes the downstream section. In this condition, the back-end blades move in high-flow turbulence.

It can be visually acknowledged that, due to the no-slip condition, the velocity along the entire length of the wall is zero. In the upstream area, the velocity distribution is uniform. The figures show that the turbine uses the fluid flow momentum, as a result, a low-speed area is generated downstream of the turbine.

Figure 14 presents the hydrodynamic forces acting on the turbine blades. Lift and drag are the fundamental hydrodynamic forces that affect the turbine blades. The tangential force is the essential force for the roll of the turbine and is likewise responsible for the evolution of the tangential acceleration. It is significant to know how hydrodynamic lift, and drag forces, affect the turbine blades at every instance of rotation. Therefore, the total tangential force affecting the turbine at each certain moment will be the sum of the lift and drag forces.

It is significant to recognize which force acts in the positive and negative direction of tangential force production. Lift force is the principal force to increase a positive tangential force that influences the blade. The effect of drag force on increasing the positive tangential force is low and can avoid. Almost all the drag force is converted to the normal force, which attempts to exert pressure on the blade. Therefore, we can conclude that the drag force is generally opposed to the driving turbine onward. As can be seen, with changes in airfoil sections, the normal force applying to the blades increases, which reduces the positive tangential force and decreases the lift force, and so the turbine power coefficient.

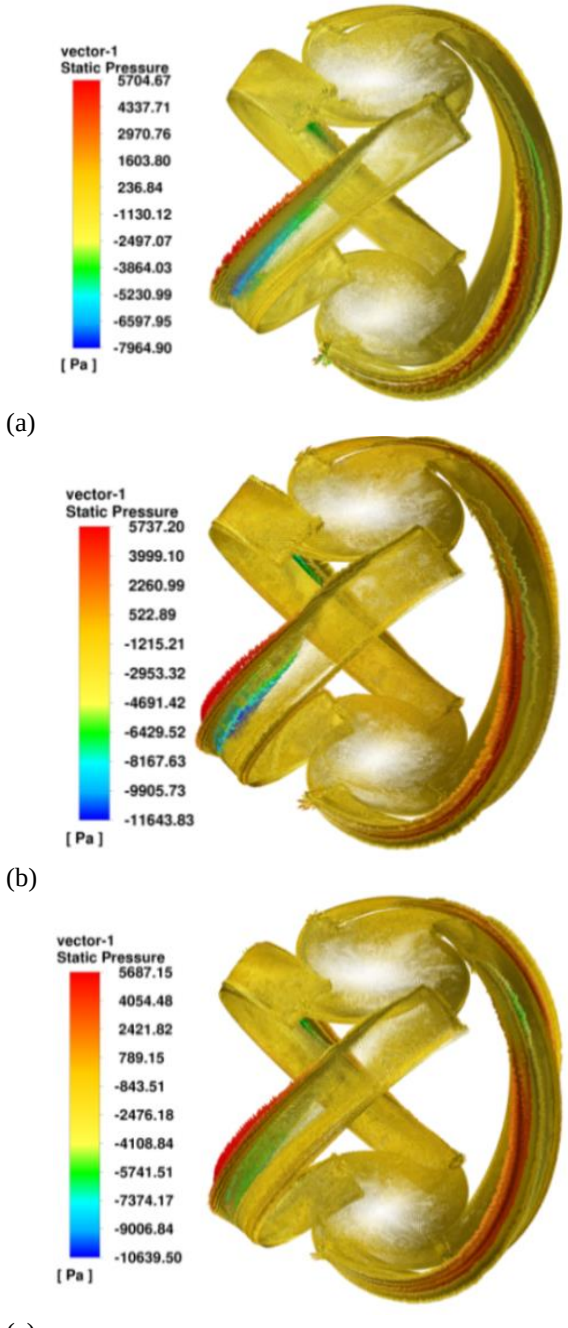

Fig. 14 Contours of static pressure near the turbine wall at λ=2.2 for (a) NACA 0020 (b) NACA 2412 and (c) NACA 64(3)418 airfoils

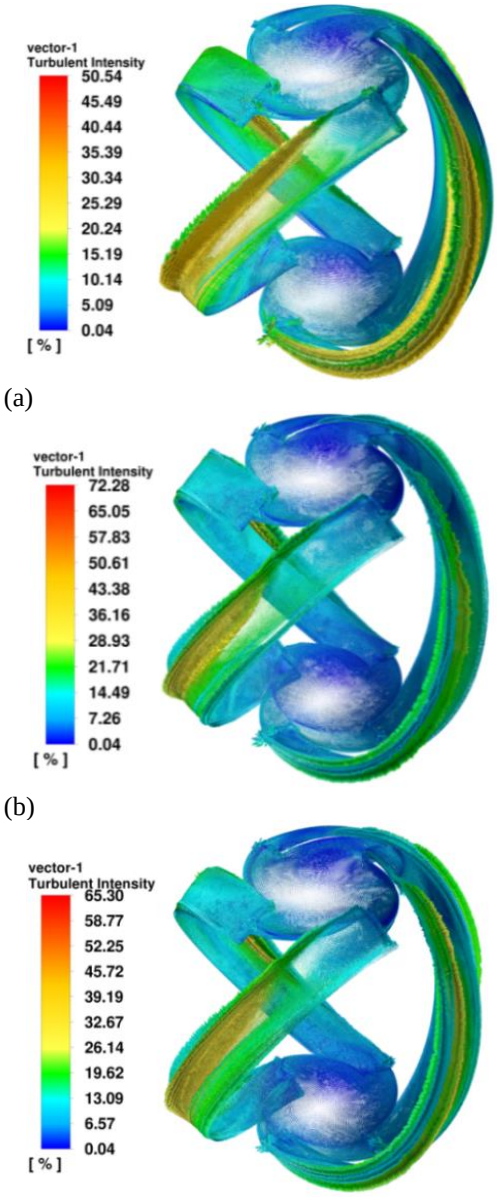

Fig. 15 Contours of turbulent intensity near the turbine walls in λ=2.2 for (a) NACA 0020 (b) NACA 2412 and (c) NACA 64(3)418 airfoils

The turbulent intensity magnitudes are presented at the blade root, leading edge, and trailing edge for different asymmetric airfoils in a three-dimensional view (Fig.15). A comparison between the turbulent intensity magnitudes shows that the flow turbulence intensity is maximum at the center of the blade. The wake flows roll up and down toward the blade tips. Turbulence mixing starts when the outer side flow initiates come into the turbulence. This type of flow movement causes wake recovery. Therefore, the flow has turbulent intensity with the minimum values around the blade trailing edge and also the hub section.

10.2 The Effect of the Different Number of Blades on the Turbine Performance

Figure 16. shows the turbines with various blade numbers. Change in the number of blades has a considerable influence on the turbine performance.

Fig. 16 Main design of the Lucid spherical turbine with different numbers of blades (a) 2 blades (b) 3 blades (c) 5 blades

The spherical lucid model turbine was examined with 2, 3, and 5 blades. Figure 17, presents that the drag and power coefficients have been used to compare with the experimental results. For the two-bladed turbine, the maximum deviation from the original turbine drag coefficient is about 31% and 34%, for NACA 2412 and NACA 64(3)418 airfoils, respectively. By subtraction of the number of blades, the decrease in turbine surface area to the inlet flow causes to drop in the power coefficient down to 91% and 92% for NACA 2412 and NACA 64(3)418 compared to the original version respectively Three-bladed turbine possesses the best results among all models. For this model, the power coefficient increased by 12% and 71% for NACA 2412 and NACA 64(3)418 sections, respectively. The maximum deviation from the original turbine drag coefficient is about 39% and 40%, respectively. For the turbine with five blades, increasing the drag coefficient causes to decrease in the power coefficient for both NACA 2412 and NACA 64(3)418 airfoils. The high-value drag coefficient as opposed to driving the turbine forward.

Figure 18, shows the distribution of the velocity in the streamwise direction in the horizontal planes, for various turbines. Due to the no-slip condition, the velocity along the entire length of the wall is zero. In the

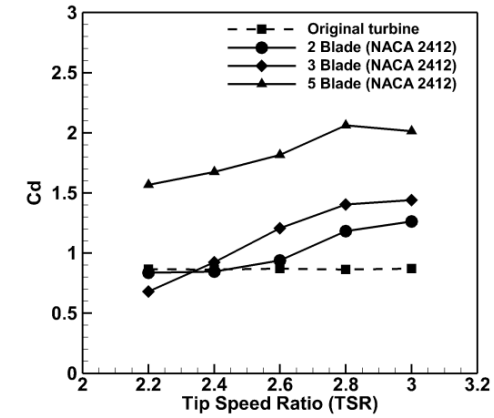

(a)

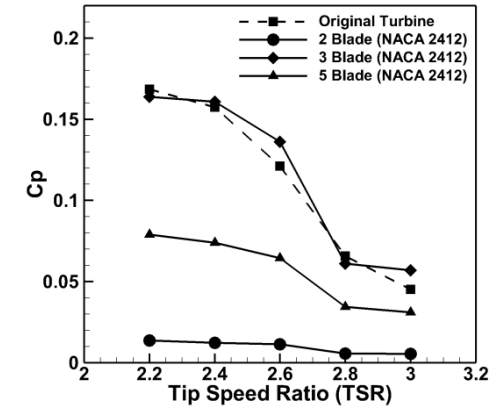

(b)

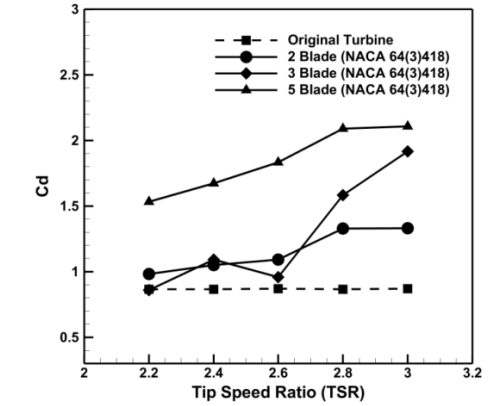

(c)

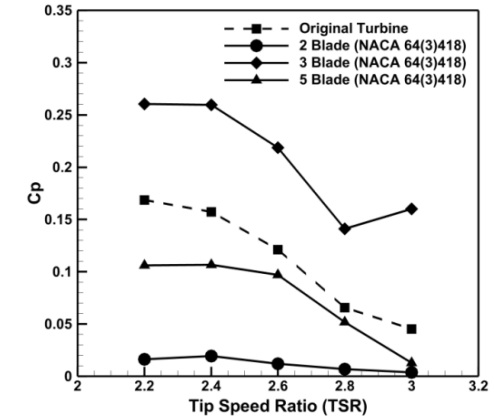

(d)

Fig. 17 Drag and power coefficient at different tip speed ratios for Lucid spherical turbine designed by a) and b) NACA 2412 and c) and d) NACA 64(3)418 airfoils Compared with the original turbine

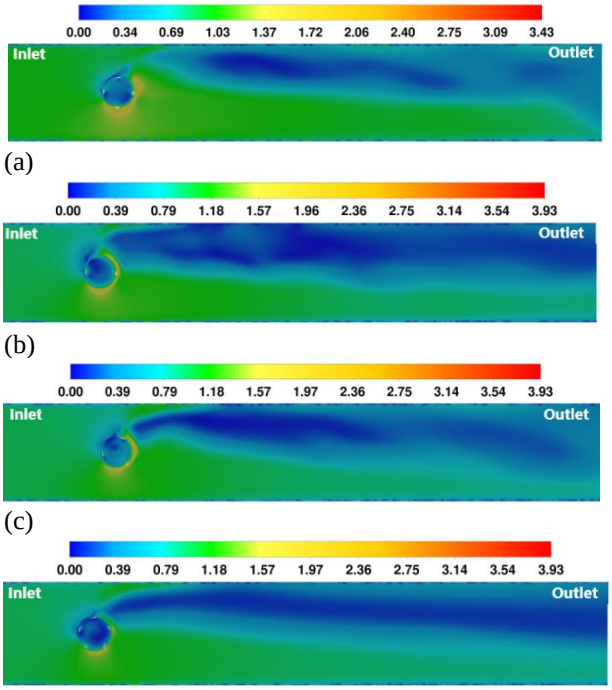

(a)

(b)

(c)

(d)

Fig. 18 Contours of streamwise velocity distribution in a horizontal plane at λ=2.2, for a turbine with a) 4 b) 2, c) 3, and d) 5 blades for NACA 643418

upstream area, the velocity distribution is considerably uniform. It is obvious, that the turbine with three blades extracts more momentum from the flow. The low-speed area at the rear of the turbine is more expanded for this model.

Figure 19 presents the hydrodynamic forces effect on turbines with various blade numbers. The pressure on the blade is at a maximum value. A high-pressure zone is developed, at the stagnation point of the blade tip, in the blade center area pressure drop to a low value and the pressure gradient is negative. Positive and negative pressure gradient area on both sides of the blade causes lift generation and blade rotation. The lift force is the main force for creating a positive tangential force on the blade compared to the drag force. The hydrodynamic forces applied to the turbine blades strongly depend on the cross-section of the airfoil and the position of the blades. For a two-bladed turbine by reduction of the number of blades, the hydrodynamic forces applied to the blades are reduced; this causes to decrease in the power coefficient. For a three-bladed turbine, due to the position of the turbine blades to the inlet flow, the normal force applied to the blades decreases, which increases the positive tangential force and increases the lift coefficient, and consequently the turbine power coefficient. The high distribution of a positive tangential force is seen in the middle of the blade in this model. For a five-bladed turbine, due to the increase in the number of blades, the normal force distribution on the blades is more uniform but the addition in blade number and obstruction of flow causes to decrease in power coefficient.

Figure 20 shows the turbulent intensity near the turbine wall. As can be seen for a two-bladed turbine, the flow turbulent intensity is maximum at around the middle

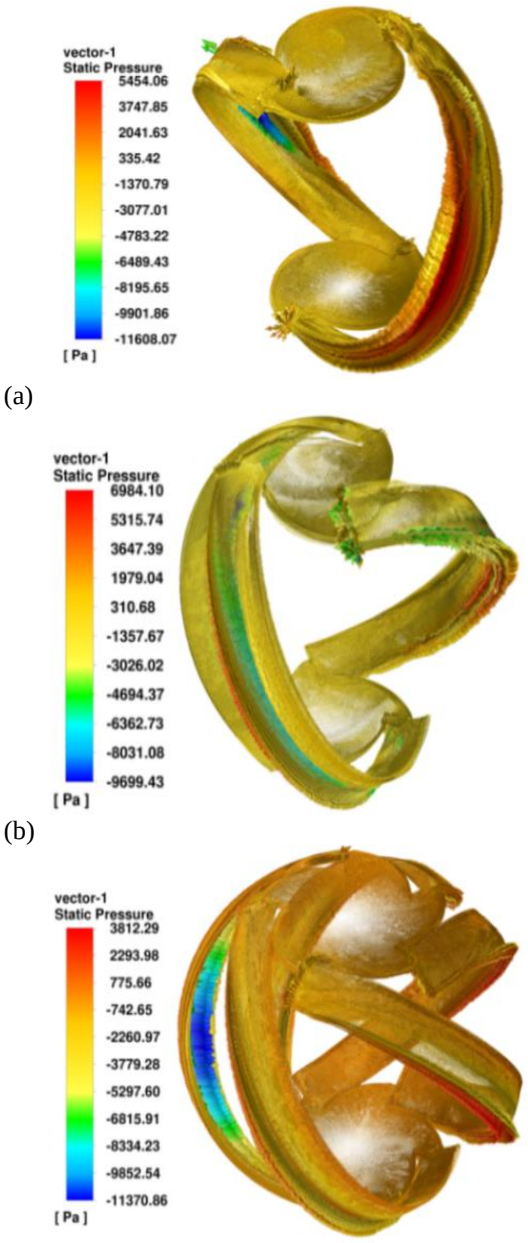

Fig. 19 Contours of static pressure near the turbine walls at λ=2.2, (a) 2 blades (b) 3 blades (c) 5 blades, for NACA 2412 section

of the blade. Poor turbulence mixing and the wake recovery cause to decrease in lift coefficient. The separation causes to increase in the thickness of the boundary layer of flow on the rear blades leading to dynamic stalls. The blades are in the deep stall, and the power coefficient drops to the minimum value. For a three-bladed turbine, wake recovery causes to increase in the lift force. Due to the position of the blades to the inflow, the blades are not in the deep stall and the lift force is at its maximum value. As a result, there is an increase in the power coefficient. For a turbine with five blades, in the front section, flow is separated from the turbine blades. This means that these blades are in the dynamic stall and the drag force is dominant, a situation that causes the lift coefficient to decrease to a lower value and so the power coefficient.

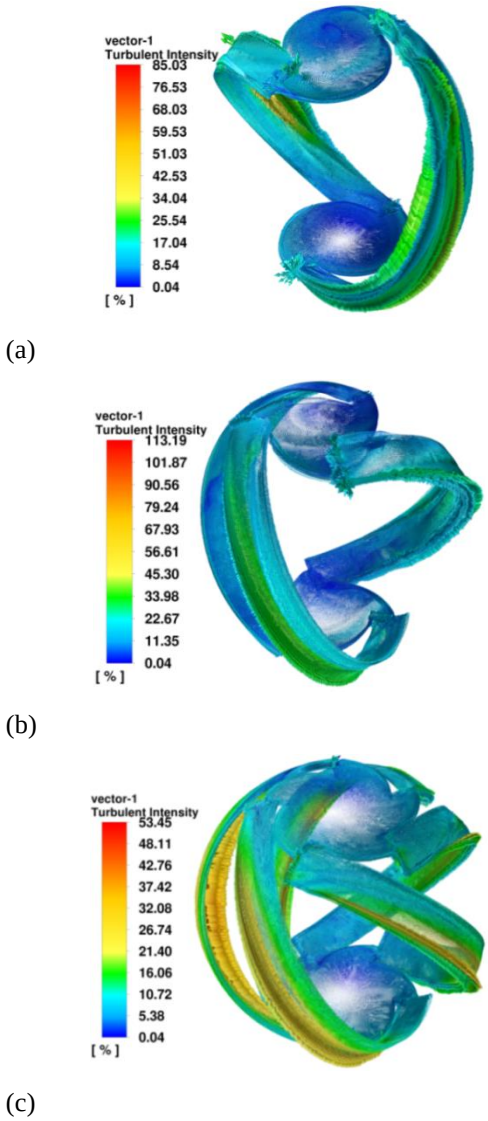

Fig. 20 Contours of turbulent intensity near the turbine walls at λ=2.2, (a) 2 blades (b) 3 blades, and (c) 5 blades, for NACA 2412 section

10.3 Twisting of Blades

Turbine blades are twisted by SolidWorks software so that the onset and end of the blades are under angles of 2, 4, -2, and -4 degrees, respectively, comparable to the inlet flow. Numerous numerical investigations were applied to evaluate and use these twist angles (Fig. 21).

As we can see in Fig. 22 the power coefficient in the different tip speed ratios at negative twist angles increased compared with the original turbine. For NACA 2412, at a twist angle of -2 degrees, the power coefficient increased to about 19%. However, at a twist angle of -4 degrees, this value increased up to 31% for NACA 643418 section. For NACA 2412 and NACA 64(3)418, the maximum deviation from the original turbine drag coefficient at twist angles of -2o and -4o is decreased. Decreasing the drag coefficient, which is opposed to driving the turbine forward, has increased the turbine power coefficient.

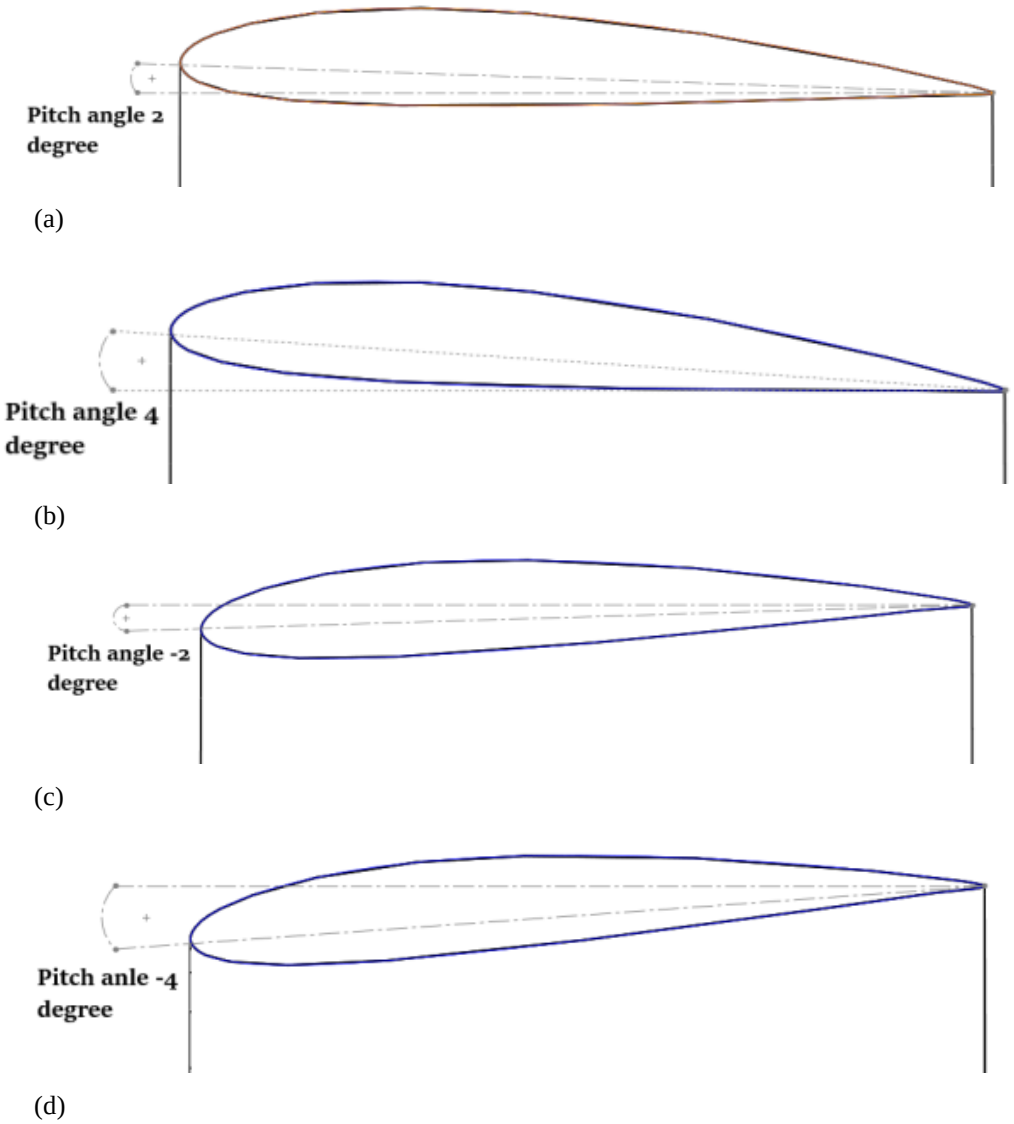

Fig. 21 Representing the twisted sections of the turbine blades in the twist angles a) 2, b) 4, c) -2, and d) -4 degrees

There is an inclination to expand the low-speed zone behind the turbine. The axial velocity of the turbulent area behind the turbine decreases. By twisting the blade to -4 degrees, the low-speed area is extra developed downstream of the turbine, which means more kinetic energy from the flow is extracted.

The lift force is fundamental for creating a positive tangential force on the blade rather than the drag force. Figure 24 shows that the blade twist angle of -4 degrees causes to gain of the positive tangential force distribution on the blades, which has increased the power coefficient of the turbine compared to the experimental test. The variation between the maximum and minimum static pressure value for a twist angle of -4 degrees is extremely higher than in other models.

Contours of turbulent intensity near the turbine wall represent that flow turbulent intensity is minimum at around the middle of the blade for negative twist angles. Twisting blades have a significant influence on the turbulence mixing and wake recovery, as it causes to increase in lift coefficient. Due to the low separation region, the thickness of the boundary layer is reduced, blades are not in the deep dynamic stall, and the lift coefficient increases to the maximum value so the power coefficient.

10.1 The Influence of the Chord Length

Results, for a turbine with a chord length of 20 cm are given in Fig.27. In addition, increasing the blade chord length by varying the speed tip ratios has a significant effect on the power coefficient. Figure 26, shows the main design of the lucid spherical turbine with a chord length of 20 cm.

Increasing the blade chord length causes to increase in power coefficient compared to the experimental test. For NACA 2412 and NACA 64(3)418 airfoils, the maximum deviation from the original turbine drag coefficient is about 31% and 34%, respectively. Due to the increasing chord length of turbine blades, the power coefficient increased by 12% for NACA 2412 in high tip speed ratios. The results are shown in Fig. 27.

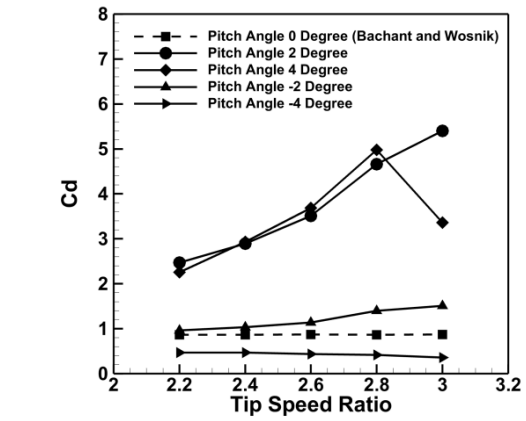

(a)

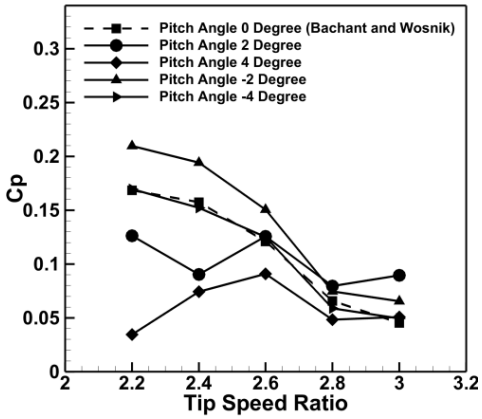

(b)

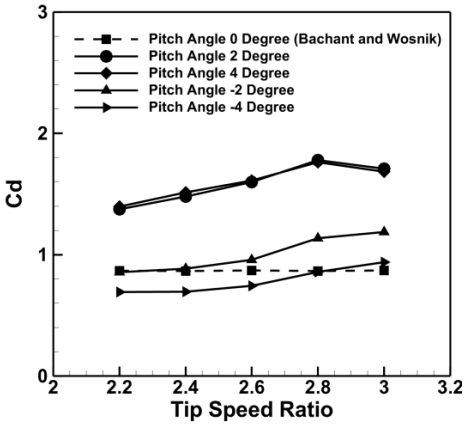

(c)

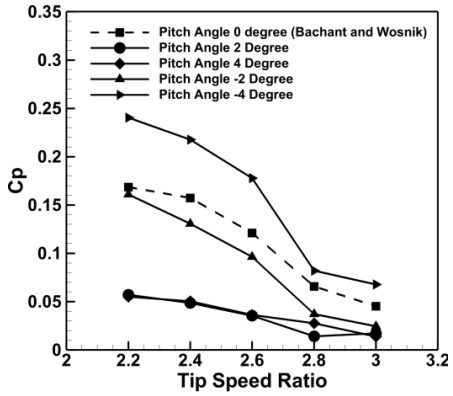

(d)

Fig. 22 (a) Drag and (b) power coefficient in various tip speed ratios for NACA 2412 and (c) drag and (d) power coefficient for NACA 64(3)418 sections at different twist angels compared with the original turbine

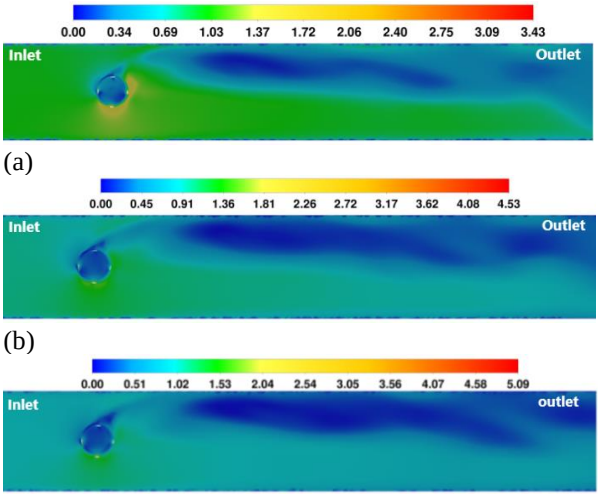

(a)

(b)

(c)

Fig. 23 Contours of streamwise velocity distribution in a horizontal plane at λ=2.2, pitch angles of a) 0 degree, b) -2 degree, and c) -4 degree

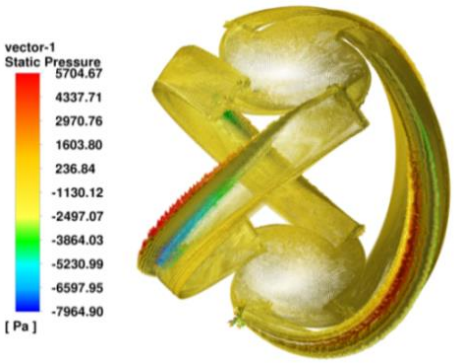

(a)

(b)

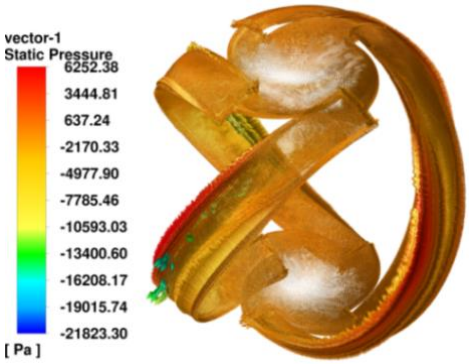

(c)

Fig. 24 Contours of static pressure near the turbine walls at λ=2.2, for twist angles of (a) 0 degree (b) -2 degrees (c) -4 degrees

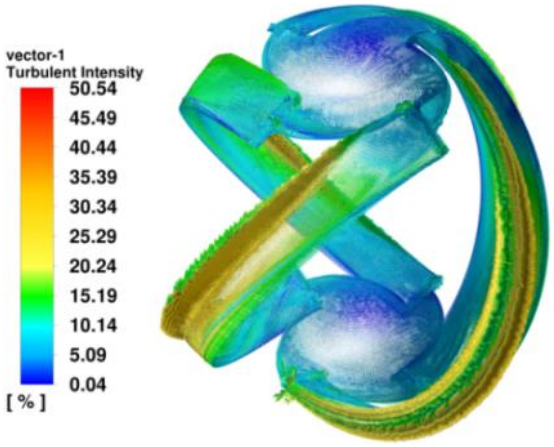

(a)

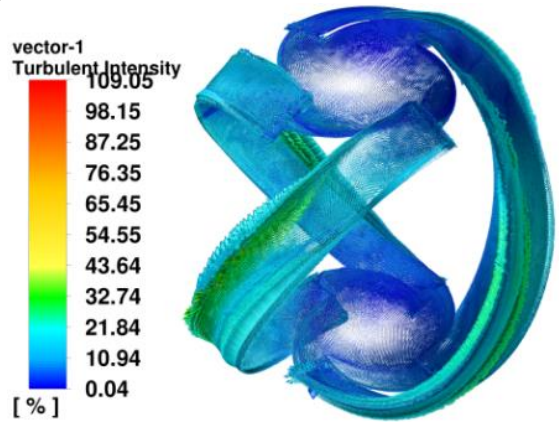

(b)

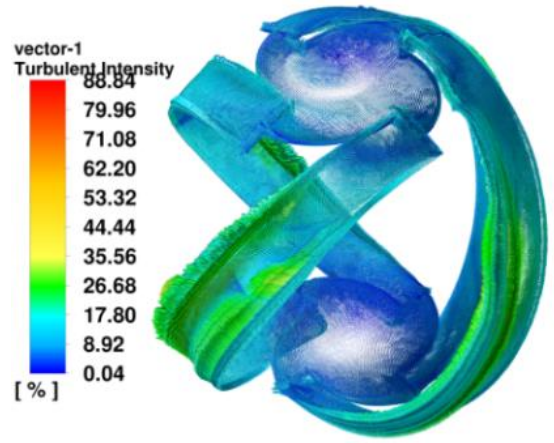

(c)

Fig. 25 Contours of turbulent intensity near turbine walls at λ=2.2, for twist angles of (a) 0 degree (b) -2 degrees (c) -4 degrees

Fig. 26 The main design of the lucid spherical turbine with a chord length of 20 cm

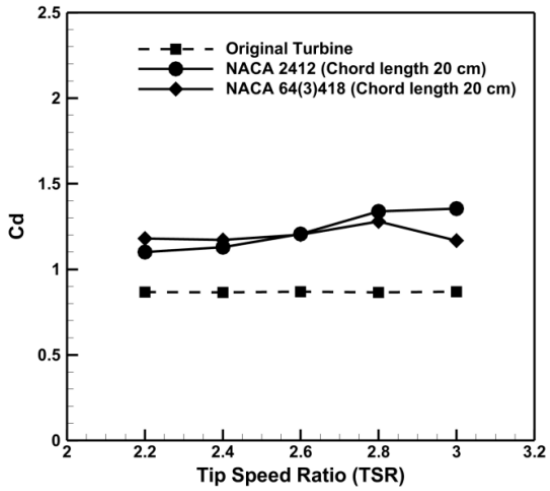

(a)

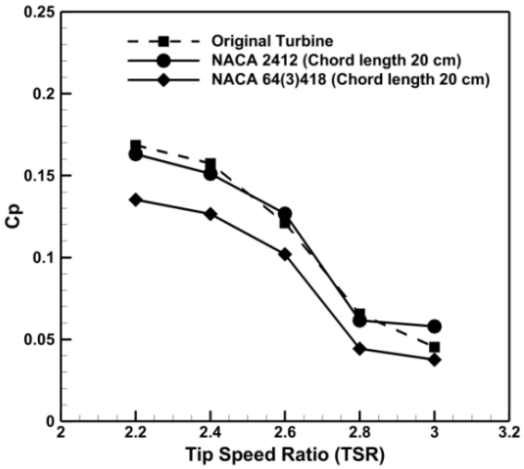

(b)

Fig. 27 (a) Drag and (b) power coefficient in various tip speed ratios for NACA 2412 and NACA 64(3)418 sections compared with the original turbine

11. CONCLUSION

The lucid spherical turbine is studied numerically. The vertical-axis turbine is installed in the water channel to supply power. In this research, the lucid spherical turbine with the different parameters of blades was designed and the external power coefficient of the turbines was measured numerically. The impact of four effective blade parameters, involving profile section type, chord length, number of blades, and blade twist, on turbine performance over a wide range of tip speed ratios, is investigated. Over a range of tip-speed ratios. The asymmetric section NACA 2412 and NACA 64(3)418 airfoils were chosen to consider the effect of the profile section. It can deduce that the power coefficient has increased up to 22% for NACA 2412 compared to the experimental test. Finally, it was found that increasing the blade chord length causes to increase in power coefficient of up to 12% for NACA 2412 section compared to the experimental test turbine. Also, if a three-bladed turbine is used, the best results are obtained by increasing the power coefficient by 12% and 71% for NACA 2412 and NACA 64(3)418 airfoils

respectively. The twist of the blades caused to increase in the power coefficient by 19% and 31% for NACA 2412 and NACA 64(3)418 sections respectively. With the inlet velocity of 1m/s and different non-dimensional tip-speed ratios using these asymmetric airfoils for blades leads to a positive effect on the turbine performance, but this subject still needs more effort and consideration. Increasing the blade chord length causes to increase in power coefficient compared to the experimental test turbine. For NACA 2412 and NACA 64(3)418 airfoils, the maximum deviation from the original turbine drag coefficient is about 31% and 34%, respectively. Due to the increasing chord length of turbine blades, the power coefficient increased by 12% for NACA 2412 in high tip speed ratios. The results are shown in Fig.27.

Overall, we can find out the three-bladed turbine has the best performance among all models and is also the original turbine that has been tested by Bachant and Wosnik. In addition, negative twisting angles and increasing chord length caused better performance rather than other models.

CONFLICTS OF INTERESTS

The authors declare that they have no conflict of interest.

AUTHORS CONTRIBUTIONS

H. Zarei: Conception and design of study, acquisition of data, analysis and/or interpretation of data, drafting the manuscript, revising the manuscript critically for important intellectual content; **M. Pasandidehfard**: Conception and design of study, analysis and/or interpretation of data, drafting the manuscript, revising the manuscript critically for important intellectual content

REFERENCES

Alaimo, A., Esposito, A., Messineo, A., Orlando, C., & Tumino, D. J. E. (2015). 3D CFD analysis of a vertical axis wind turbine. *Energies*, *8*(4), 3013-3033. https://doi.org/10.1177/1475090211400684

Antheaume, S., Maître, T., & Achard, J. L. J. R. E. (2008). Hydraulic Darrieus turbines efficiency for free fluid flow conditions versus power farms conditions. *Renewable Energy*, *33*(10), 2186-2198. https://doi.org/10.1016/j.renene.2007.12.022

Bachant, P., & Wosnik, M. J. R. E. (2015). Performance measurements of cylindrical-and spherical-helical cross-flow marine hydrokinetic turbines, with estimates of exergy efficiency. *Renewable Energy*, *74*, 318-325. https://doi.org/10.1016/j.renene.2014.07.049

Balduzzi, F., Zini, M., Molina, A. C., Bartoli, G., De Troyer, T., Runacres, M. C., Bianchini, A. (2020). Understanding the aerodynamic behavior and energy conversion capability of small darrieus vertical axis wind turbines in turbulent flows. *Energies*, *13*(11), 2936. https://doi.org/10.3390/en13112936

Carlton, J. (2018). *Marine propellers and propulsion*. Butterworth-Heinemann.

Castelli, M. R., Dal Monte, A., Quaresimin, M., & Benini, E. J. R. E. (2013). Numerical evaluation of aerodynamic and inertial contributions to Darrieus wind turbine blade deformation. *Renewable Energy*, *51*, 101-112. https://doi.org/10.1016/j.renene.2012.07.025

Dashti Mahmoud-Abadi, B., Zareei, H., Pasandidehfard, M. J. J. O. S., & Mechanics, F. (2022). Numerical simulation of Lucid spherical turbine and investigation the effect of different parameters of blades on its performance. *Journal of Solid and Fluid Mechanics*, *12*(1), 115-131. https://doi.org/10.22044/jsfm.2022.9993.3346

El Chazly, N. J. R. E. (1993). Static and dynamic analysis of wind turbine blades using the finite element method. *Renewable Energy*, *3*(6-7), 705-724. https://doi.org/10.1016/0960-1481(93)90078-U

Furukawa, A., Takamatsu, Y., Okuma, K., & Takenouchi, K. J. (1992). Optimum design of the Darrieus-type cross flow water turbine for low head water power. *Renewable Energy, Technology and the Environment* 2824-2828. https://doi.org/10.1016/b978-0-08-041268-9.50078-x

Ghiasi, P., Najafi, G., Ghobadian, B., Jafari, A., & Mazlan, M. J. S. (2022). Analytical study of the impact of solidity, chord length, number of blades, aspect ratio and airfoil type on h-rotor darrieus wind turbine performance at low reynolds number. *Sustainability*, *14*(5), 2623. https://doi.org/10.3390/su14052623

Gorle, J., Chatellier, L., Pons, F., & Ba, M. (2015). *Critical Analysis of the Effectiveness of Blade Pitching for Vertical Axis Water Turbine.* Paper presented at the 11th European Wave and Tidal Energy Conference Series (EWTEC).

Hellsten, A., Laine, S., Hellsten, A., & Laine, S. (1997). *Extension of the k-omega-SST turbulence model for flows over rough surfaces.* Paper presented at the 22nd atmospheric flight mechanics conference. https://doi.org/10.2514/6.1997-3577

Hohman, T., Martinelli, L., Smits, A. J. J. O. W. E., & Aerodynamics, I. (2018). The effects of inflow conditions on vertical axis wind turbine wake structure and performance. *Journal of Wind Engineering and Industrial Aerodynamics*, *183*, 1-18. https://doi.org/10.1016/j.jweia.2018.10.002

Hwang, I. S., Lee, Y. H., & Kim, S. J. J. A. E. (2009). Optimization of cycloidal water turbine and the performance improvement by individual blade control. *Applied Energy*, *86*(9), 1532-1540. https://doi.org/10.1016/j.apenergy.2008.11.009

Li, Q., Cai, C., Maeda, T., Kamada, Y., Shimizu, K., Dong, Y., Xu, J. (2021). Visualization of

aerodynamic forces and flow field on a straight-bladed vertical axis wind turbine by wind tunnel experiments and panel method. *Energy*, *225*, 120274. https://doi.org/10.1016/j.energy.2021.120274

Manwell, J. F., McGowan, J. G., & Rogers, A. L. (2010). *Wind energy explained: theory, design and application*. John Wiley & Sons.

Moghimi, M., & Motawej, H. J. J. O. A. F. M. (2020). Comparison Aerodynamic Performance and Power Fluctuation Between Darrieus Straight-Bladed and Gorlov Vertical Axis Wind Turbines. *Journal of Applied Fluid Mechanics*, *13*(5), 1623-1633. https://doi.org/10.36884/jafm.13.05.30833

Paillard, B., Hauville, F., & Astolfi, J. A. J. R. E. (2013). Simulating variable pitch crossflow water turbines: A coupled unsteady ONERA-EDLIN model and streamtube model. *Renewable Energy*, *52*, 209-217. https://doi.org/10.1016/j.renene.2012.10.018

Shimokawa, K., Furukawa, A., Okuma, K., Matsushita, D., & Watanabe, S. J. R. E. (2012). Experimental study on simplification of Darrieus-type hydro turbine with inlet nozzle for extra-low head hydropower utilization. *Renewable Energy*, *41*, 376-382. https://doi.org/10.1016/j.renene.2011.09.017

Tunio, I. A., Shah, M. A., Hussain, T., Harijan, K., Mirjat, N. H., & Memon, A. H. J. R. E. (2020). Investigation of duct augmented system effect on the overall performance of straight blade Darrieus hydrokinetic turbine. *Renewable Energy*, *153*, 143-154. https://doi.org/10.1016/j.renene.2020.02.012

Yang, W., Hou, Y., Jia, H., Liu, B., & Xiao, R. J. E. (2019). Lift-type and drag-type hydro turbine with vertical axis for power generation from water pipelines. *Energy*, *188*, 116070. https://doi.org/10.1016/j.energy.2019.116070